Weld World (2016) 60:883–897
DOI 10.1007/s40194-016-0348-2

RESEARCH PAPER

Micromechanical characterisation of weld metal susceptibility to hydrogen-assisted cold cracking using instrumented indentation

Rahim Kurji[1] · **Olivier Lavigne**[1] · **Reza Ghomashchi**[1]

Received: 1 February 2016 / Accepted: 18 April 2016 / Published online: 25 April 2016

Abstract Hydrogen-assisted cold cracking is generally accepted to be the consequence of a critical concentration of hydrogen trapped within a susceptible microstructure and subjected to a threshold level of stress. Traditionally, hardness has been used as a proxy for establishing the critical limits above which the risk of a hydrogen crack propagating is considered significant. However, developments in the steel-making process, in particular thermomechanically controlled processing, has brought into question the suitability of empirical hardness limits developed using older generation steels. In this paper, a safe welding boundary was established for single-pass root runs for API 5 L X70 steel welded with E6010 electrodes. Across this boundary, it was shown that hydrogen cracks were present in welds with hardness's well below the traditionally accepted threshold of 350 HV. This paper explores the use of nanoindentation as means of quantifying the susceptibility of welds deposited on high-strength low-alloy steels, using shielded metal arc welding, to hydrogen-assisted cold cracking. It is suggested that the use of the hardness/elastic modulus (H/E) ratio, which is directly related to the yield strength of a material, is a more suitable parameter to predict weld metal hydrogen-assisted cold cracking (HACC) susceptibility than is the hardness alone.

Keywords (IIW Thesaurus) Pipeline steels · MMA welding · Cold cracking · Hardness · Elasticity

Recommended for publication by Study Group RES - Welding Research Strategy and Collaboration

✉ Olivier Lavigne
Olivier.lavigne@adelaide.edu.au; lavigneolivier@hotmail.com

[1] School of Mechanical Engineering, The University of Adelaide, Adelaide, SA 5005, Australia

1 Introduction

In Australia, the use of hydrogen-rich cellulosic consumables is common place for the construction of oil and gas pipeline networks. Coupled with the high levels of restraint as a result of clamping and the lifting-lowering stresses, the pipeline is subjected to during construction, the root pass is generally accepted as the most vulnerable pass with respect to susceptibly to hydrogen-assisted cold cracking (HACC). Although the exact mechanism governing the initiation and propagation of hydrogen cracks is still in contention, it is generally accepted that hydrogen cracks occur when critical levels of hydrogen interact with a susceptible microstructure when a weld is subjected to a threshold level of stress [1–20]. Preheat can minimise the risk of cracking [2–4]; however, it limits weld productivity and adds costs. To ensure that the risk of HACC is designed out of the weld procedure, evaluation of the conditions for the onset of HACC needs to be established with confidence.

1.1 Weld metal hydrogen-assisted cold cracking

Hydrogen cracking is traditionally associated with crack initiation and propagation through the heat-affected zone (HAZ). However, with the improvements in the steel-making process and a consequent reduction in steel hardenability, an increased tendency for HACC to occur in the weld metal (WM) rather than the HAZ is suggested [3, 17, 21, 22]. The prevalence of weld metal hydrogen-assisted cold cracking (WMHACC) over heat-affected zone hydrogen cracking (HAZ HACC) has been suggested to be the consequence of changes in the alloy content and the as-cast microstructure of the parent plate. Modern alloy designs have raised the austenite (γ) to ferrite (α) transformation temperatures of the heat-affected zone to a point where the ferrite transformation occurs in the heat-

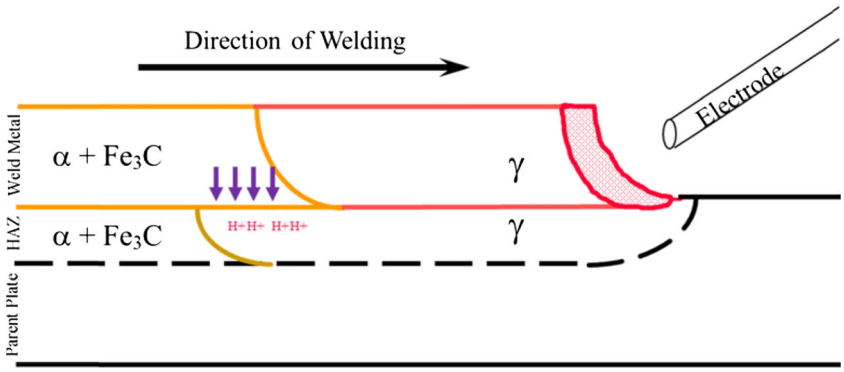

Fig. 1 HAZ-HACC. The austenite (γ) to ferrite (α) transformation is suggested to occur in the WM before the HAZ, leaving the HAZ to effectively acting as a hydrogen sink. Hydrogen accumulates in areas of high tri-axial stress within the HAZ, creating conditions which favour the formation of hydrogen cracks

affected zone before the weld metal [1]. As the solubility of hydrogen in ferrite is lower than in austenite [23], hydrogen is rejected from the HAZ and accumulated in the WM. The higher diffusivity of hydrogen in ferrite [24] also favours this process. The consequence is the preferential accumulation of hydrogen in the weld metal as illustrated in Figs. 1 and 2.

1.2 Predicting the onset of hydrogen-assisted cold cracking—HACC control criterions

The potential catastrophic consequence of hydrogen-assisted cold cracking has seen a significant amount of research focused on deriving methods to predict the onset of the phenomenon. As it universally agreed [1–22, 25–27], that HACC can be summed up as the critical interaction of three factors (hydrogen concentration, susceptible microstructure and stress), empirical predictors have generally focused on identifying thresholds of the three factors above which the risk of HACC is considered to be significant.

Considering that an accurate estimation of stresses evolved during fabrication is difficult to achieve, the most commonly adopted methods by industry and in particular by statutory codes is the control of hydrogen and a control of the resulting microstructure. Unlike residual hydrogen which has a direct correlation to the level of preheat applied [2] and thus makes the hydrogen control criterion the most commonly adopted control criterion, a proxy which defines a 'susceptible' microstructure is much more complex to define. The complexity arises from the inhomogeneity of the weld microstructure [28].

The simplest proxy used to define microstructural susceptibility to hydrogen cracking is hardness [2–4, 17]. It is therefore not surprising that hardness control criterions have been extensively codified [29–31]. Graville [19] compared the suitability of the hardness versus the hydrogen control criterions and suggested that the use of hardness control is best suited to steels with limited alloy content. His hypothesis was based on the observation that steels with a limited alloying content have steep hardening curves and the hardness of the heat-affected zone can be determined with a high degree of accuracy by measuring the critical cooling time ($t_{8/5}$; Fig. 3). Conversely, for low-carbon and microalloyed steels, as the hardness profile of the weld is not influenced significantly by the critical cooling time ($t_{8/5}$), Graville suggested that hydrogen control approach would be more appropriate.

Based on empirical observations, a system commonly known as Graville's diagram (Fig. 4), which classifies steels based on their carbon content and alloying constituents, was proposed. This system simplifies the selection of the most appropriate criterion to employ to minimise the risk of hydrogen cracking.

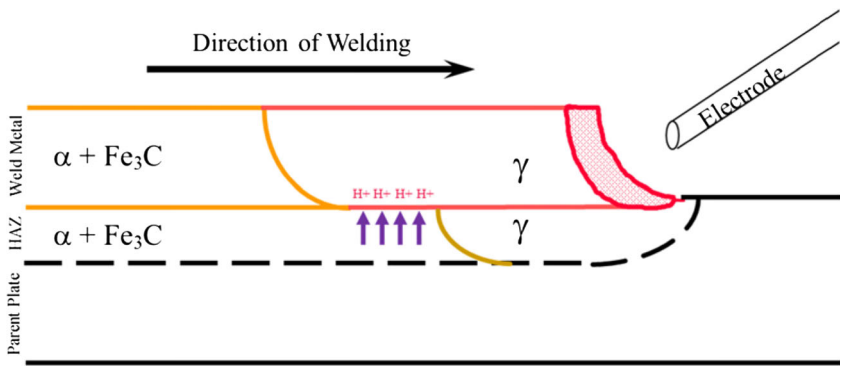

Fig. 2 WM-HACC. Modern alloy designs favour the austenite (γ) to ferrite (α) transformation in the HAZ before the WM. This transforms the WM into an effective hydrogen sink within which hydrogen can accumulate in areas of high tri-axial stress, creating the conditions which favour the formation of hydrogen cracks

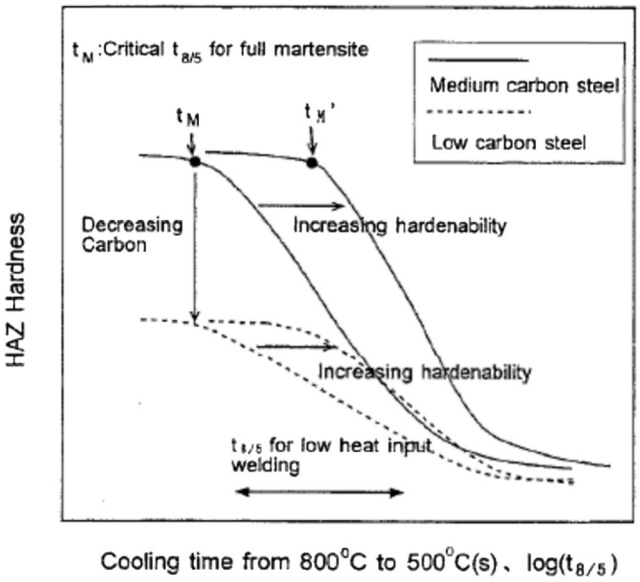

Fig. 3 Schematic representation of hardenability curves for low- and medium-carbon steels [4]. HAZ hardness of medium-carbon steels change significantly in a $t_{8/5}$ region corresponding to low heat input welding or when the carbon equivalent changes (CE_{IIW})

Zone 1 steels are typically considered to be steels at low risk of cracking, unless welded under high restraint and with high-hydrogen electrodes such as cellulosic electrodes. When considering HACC control strategies to implement, steels in zone I are typically subject to the hydrogen control criterions. Zone 2 steels on the other hand are characterised by significantly higher-carbon content and consequently have much steeper hardening curved compared to steels in zone 1. Steels in zone 2 are therefore subject to hardness control criterions. Zone 3 steels are typically subject to a combination of both criterions given the elevated risk of cold cracking.

It is important to note that the hydrogen and the hardness control criterions have different areas of emphasis. As

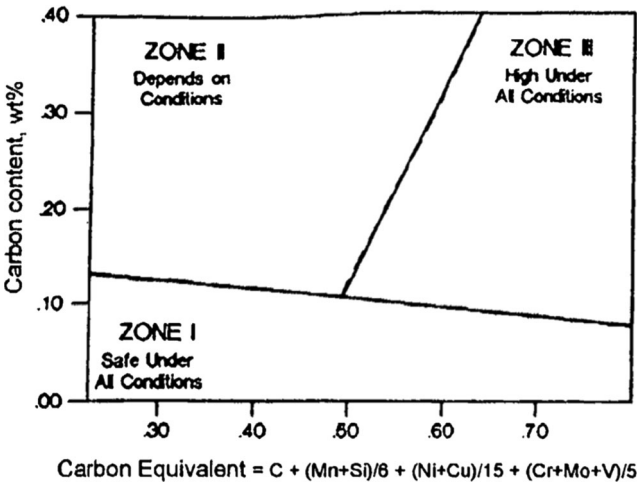

Fig. 4 Graville's diagram [19], illustrating the classification of steel weldability based on their carbon content and alloying composition as described by their carbon equivalent

expected, with hydrogen control criterions, the emphasis is on hydrogen diffusion and restraint, whereas with hardness control criterion, the emphasis is on the primary factor which influences the resulting microstructure, namely chemistry. Nevertheless, both control criterions acknowledge and take into consideration that HACC is the consequence of the interaction of trapped hydrogen in a susceptible microstructure subject to stress when estimating the level of preheat required to ensure that crack-free welds can be deposited.

The introduction of new microalloyed, thermomechanically controlled processed (TMCP) steels has raised the question of the suitability of the empirically derived control criterions, based on older generation steels. Limited data on the suitability of these traditional criterions on newer grades of steels and studies such as those by Davison et al. [32] demonstrate the need to assess the control criterions. This is compounded by the development of novel methods which can be used to extract mechanical properties of materials such as instrumented indentation.

1.3 Instrumented indention

Although indentation has been used to measure hardness for several decades [33], technological advancement in the field of instrumentation and the subsequent advent of instrumented indention, on both at microscale and nanoscale, have facilitated the measurement of material micromechanical properties through the decomposition and analysis of the load versus penetration depth curve. Numerous reviews addressing the fundamental principles of contact mechanics upon which the technique of instrumentation indentation is based have been published in addition to reviews exploring the applications of instrumented indention [33–42].

Unlike classical hardness measurements which use a definite test body to make an indent into the surface of a material, which has to be optically measured, instrumented indentation utilises an accurate measurement of the load applied to the indenter tip and the consequent depth of penetration into the surface. This allows for an accurate measurement of the universal hardness, H, as highlighted in Eq. 1, where F_{max} is the maximum applied load and A_c is the cross-sectional area corresponding to the depth h_c.

$$H = \frac{F_{\max}}{A_C(h_c)} \tag{1}$$

The determination of the contact depth h_c is given by Eq. 2, where S is the contact stiffness obtained from the slope of the upper portion of the unloading force-depth curve (Eq. 3).

$$h_c = h_{\max} - 0.75\frac{F_{\max}}{S} \tag{2}$$

Table 1 Divisions of the experimental program

Tier 1	Weldability tests are conducted to derive an empirical envelope within which a safe welding boundary can be delineated.
Tier 2	Samples selected from across the derived safe weld boundary are characterised using instrumented indentation to determine the elastic modulus and hardness of weld metal microstructure.

$$S = \frac{dF}{dh} \tag{3}$$

The reduced Young's modulus E_r which is a measure of the elastic properties of the sample can be calculated from the force-depth curves according to Eq. 4.

$$E_r = \frac{1}{2}\sqrt{\frac{\pi}{A_c(h_c)}}\frac{dF}{dh} \tag{4}$$

For an elastically deformable indenter, the reduced modulus E_r is related to the actual Young's modulus E by Eq. 5, where ν is Poisson's ratio of the indented material and ν_i and E_i are the Poisson's ratio and Young's modulus of the indenter, respectively.

$$\frac{1}{E_r} = \frac{1-\upsilon^2}{E} + \frac{1-\upsilon_i^2}{E_i} \tag{5}$$

where penetration depths are greater than 320 nm and the area function can be estimated using a standard calibration procedure on a fused silica quartz sample of a known Young's modulus [40].

Therefore, the application of instrumented indention allows for the elastic and plastic contribution to indention to be measured. This allows for the material to be characterised in terms of its elasto-plastic properties and was cited by several authors as an ideal method to characterise microstructures of steels and weld areas [40–42]. This is especially important when quantifying the susceptibility of a weld to HACC, as crack propagation is dependent on the elasto-plastic properties of the material within which a crack has initiated [43].

2 Experimental procedure

In order to establish the viability of micromechanical characterisation as a means of assessing the susceptibility of a weld deposit to HACC, a two-tier experimental program was employed as summarised in Table 1 below.

Using the two-tier approach, the variation in the key micromechanical properties can be used as a means of characterising the susceptibility to WMHACC.

2.1 Weldability testing

Weldability tests were conducted using the Modified Welding Institute of Canada (MWIC) weldability test [44] on two thicknesses (20 and 10 mm) of API 5 L X70 line pipe steel using 4-mm Ø E6010 electrodes. The MWIC test is a variant of the Welding Institute of Canada Test (WIC) which is a widely accepted weldability test used by the pipeline industry to rank the susceptibility of a single-pass weld to HACC. Figure 5 illustrates the dimensions of the test specimen and specifications of the preparation of the single butt V grove joint within which the tests welds are deposited. The elemental compositions of the batch of steel and batch of electrode used for testing are given in Tables 2 and 3, respectively. To replicate conditions found in Australia, in particular the high travel speeds, weldability testing was conducted within the parameters listed in Table 4.

To minimise variability introduced by the manual welding process, the tests welds were deposited using a

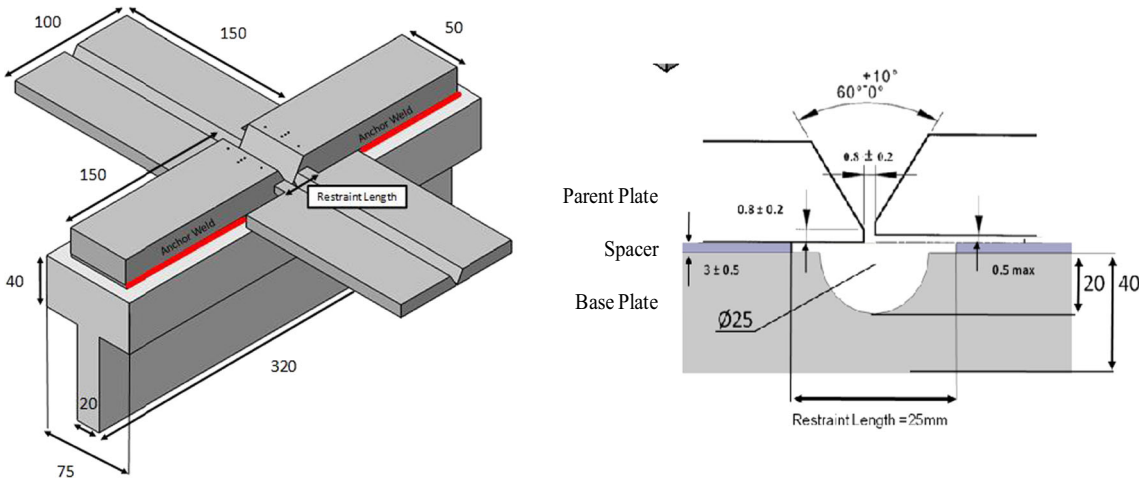

Fig. 5 Dimensions of the MWIC weldability test and single V butt weld preparation used for weldability testing. All dimensions in millimeter

Table 2 Chemical composition of line pipe steel (percent weight; from manufacturer)

C	Mn	Si	S	P	Nb	Ti	Cu	Ni	Mo	Cr	Ca	Al	V
0.052	1.55	0.21	0.0011	0.0097	0.041	0.012	0.15	0.19	0.18	0.026	0.0016	0.039	0.029

Table 3 Electrode batch chemical composition (percent weight; from manufacturer)

C	Mn	Si	S	P	Ni	Mo	Cr	V
0.16	0.62	0.19	0.009	0.009	0.2	0.01	0.02	<0.01

uni-directional, semi-mechanised shielded metal arc welding (SMAW; weld efficiency $\eta \approx 1$) machine with a specimen-holding plate moving vertically upwards during welding at a controlled velocity, thus simulating vertical-down welding conditions. A constant force and an angle of 20° normal to the plate were maintained between the electrode and the workpiece. The Lincoln Electric Invertec 350 V Pro was used as the welding power source. The groove surfaces of the test specimen and 25 mm either side of the weld centreline was polished down with ISO 80-grit (201 μm) emery paper and degreased with acetone, to minimise the probability of introducing contaminants (such as surface oil and grease) which may dissociate in the welding arc and may alter the cracking results. The entire specimen was de-gaussed prior to welding to eliminate any residual magnetic fields introduced during fabrication of the weldability specimen. This was shown to be essential [44] to ensure successful, symmetric deposition when using a semi-mechanised method of deposition on the MWIC test. Weldability testing was conducted over a 12-month period in an indoor facility where the temperature varied from a minimum of 22.6 °C to a maximum of 28.3 °C with a mean temperature of 25.1 °C. The relative humidity on site during testing varied between 38 and 67 % with a mean relative humidity of 54.1 %. The 350-mm-long, 4-mm Ø E6010 electrodes used for testing were stored in a hermetically sealed container and were used in their 'as-received' condition for testing.

2.2 Data acquisition

Welding parameter trace data (voltage and current) was collected at 0.5 Hz directly from the welding power source (Lincoln Invertec 350 V Pro) using a serial interface and the propriety software, Power Wave Manager™ supplied by Lincoln Electric. Travel speed data was derived by measuring the displacement of the specimen holding plate using Sick Laser sensor DT20-P214B (±1 mm) and the internal clock of the data acquisition system. Test plate thermal data was obtained by fitting three electrically grounded K-type thermocouples (1-mm outer diameter) coated with thermal paste into the parent plate MWIC specimen. Data was channelled at 10 Hz through an optical isolation system into several 16-bit National Instruments® (NI) 9215 voltage modules embedded in a NI-CDAQ-9188 chassis. Independent calibration was carried out to ensure signal accuracy and fidelity. A custom program was written in LabVIEW® 2010 to acquire and record data.

2.3 Weld analysis

The welded joint was removed from the MWIC specimen 24 h after weld completion by milling the test assembly just inside the restraint length. The anchor welds were sawed off using a water-cooled precision metallographic saw, and the test sample was divided into six sections. To prepare the sections for metallographic analysis and indentation, each section was hot mounted in a conductive epoxy and polished using a semi-automatic LaboForce polishing machine (Struers). Final polishing was achieved using a porous neoprene disc with a colloidal silica suspension (0.04 μm). The samples were then observed at ×400 magnification for the presence of cracking using an optical microscope (Ziess Axio Imager 2). Selected samples were then etched using a 2 % nital solution to reveal the weld metal microstructure.

Table 4 Testing parameters

Welding specifications		Welding parameters	
Direction	Vertical down (5 G)	Current	130–170 A
Size of electrode	4.0 mm	Voltage	25–30 V
AWS class	5.1 A	Travel speed	250–470 mm/min
Specification	6010 E	Heat input range (targeted)	0.41–1.00 kJ/mm
Polarity	DC+	Preheat range (targeted)	25 °C–100 °C

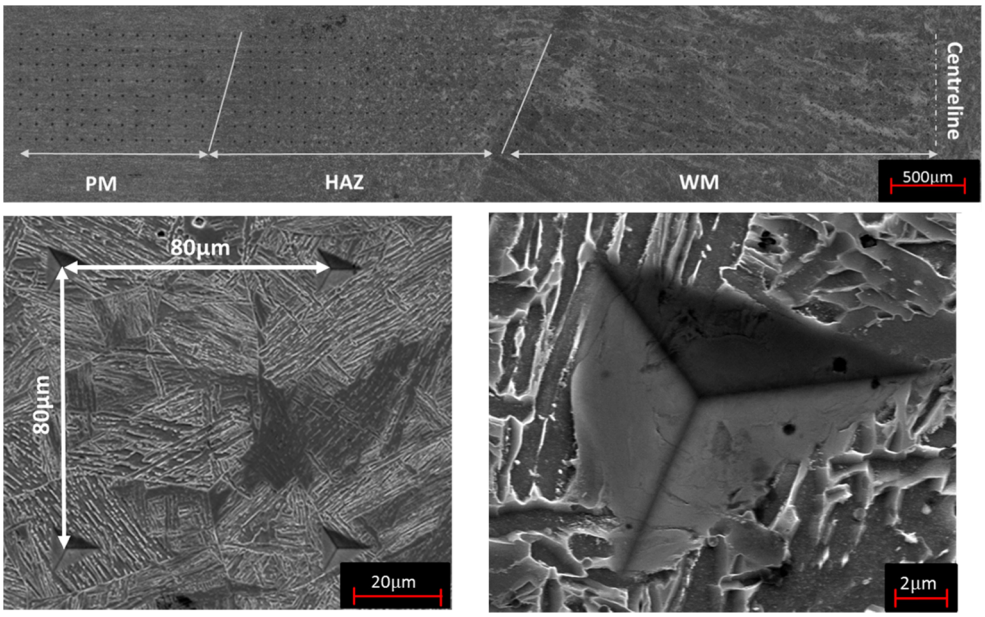

Fig. 6 *top* Indention map. *bottom left* Spacing between successive indents. *bottom right* High-magnification image of individual indent

2.4 Micromechanical analysis

For micromechanical characterisation, the fourth sections of selected test samples were prepared by mounting the metallographically prepared sample onto a sturdy test stage. The samples were attached to the stage using an adhesive to ensure no lateral movement was possible during the stage motion whilst ensuring that the test section remained perpendicular to the indenter during testing.

Indentation testing was carried out using the Fisher-Cripps IBIS Nanoindention System. Symmetric indention maps (Fig. 6), consisting of 480 indents (60 columns and 8 rows) with an 80-µm space between the centre point of each indent, were made using a Berkovich-type diamond tip indenter. The initial column was located at the approximate centreline of the weld, and the maps spanned outwards towards the HAZ. Testing was conducted at a load of 250 mN to achieve a sufficient penetration of the indenter tip into the material (approximately 2 µm). This depth insured that the tested material volume is representative of the considered microstructure volume. The area function was approximated by a standard calibration procedure with fused quartz material of known Young's modulus and hardness. High-magnification images of selected cracks, indents, and microstructure were taken using the FEI Quanta 450 FEG environmental scanning electron microscope (ESEM).

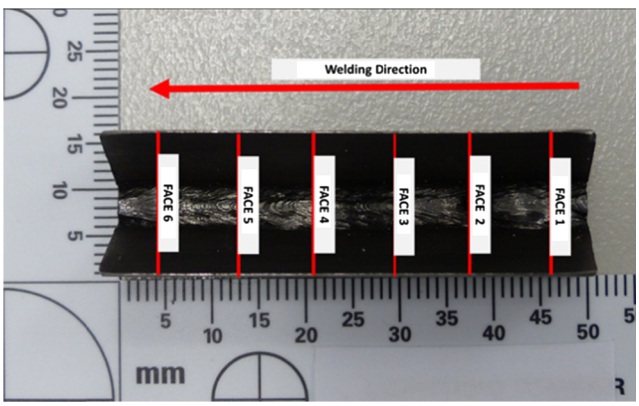

Fig. 7 Weldability test piece with the location of the six faces to be examined under an optical microscope at a magnification of ×400 highlighted

3 Results and discussion

3.1 Delineation of safe welding boundary

Each of the six sections (Fig. 7) from a single test piece was examined at a magnification of ×400 and classified as cracked when the vertical length of the defect observed in a single section (t_c) was greater than 5 % of the height of the weld bead (t_w) of the test section under analysis (Fig. 8). Cracking

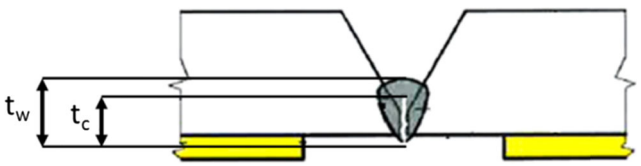

Fig. 8 Schematic of a face of a test section. A sample is defined as cracked when a linear defect whose vertical length (t_c) is greater than 5 % of the bead height (t_w)

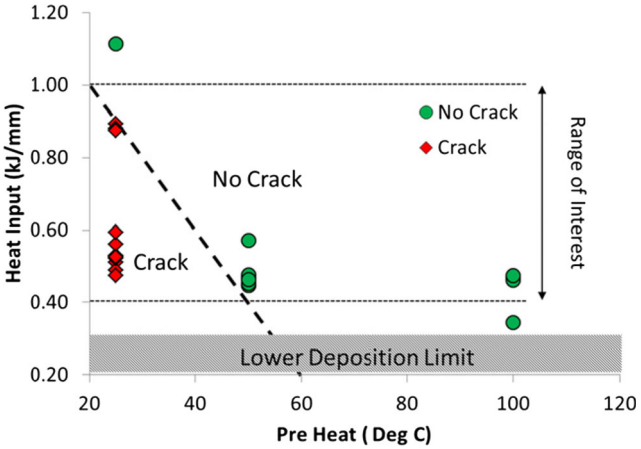

Fig. 9 MWIC weldability testing on the 20-mm-thick API 5 L X70 line pipe steel under high restraint (R_f=25 mm). A *green circle* represents a sample within which no cracking is observed. A *red diamond* represents a sample within which a crack was observed

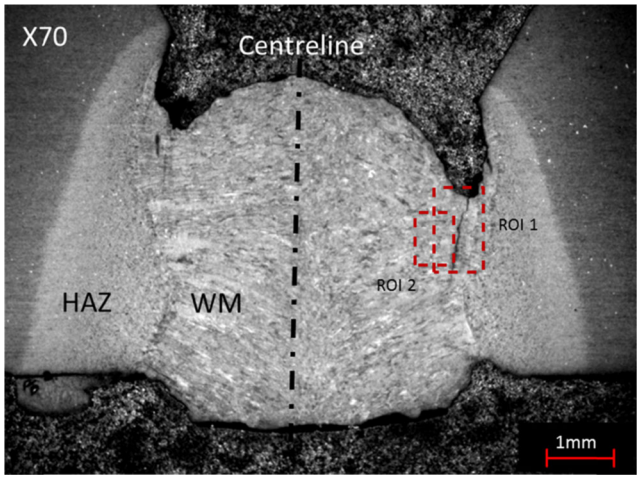

Fig. 11 Overview of weld bead (2 % nital etch) highlighting macrohydrogen (ROI 1) cracks which initiate from macroscopic defects such undercut in the weld toe and microscopic hydrogen cracks (ROI 2) which initiate from microvoids or non-metallic inclusions

severity was defined as the arithmetic sum of the observed percent cracking over the entire test piece.

A total of 25 tests were conducted for 20-mm-thick plates under high restraint (R_f=25 mm), of which 22 were used for crack analysis and 3 were used to defined the lower limit of weld deposition. For the tests used for crack analysis, the recorded current ranged from 121 to 167 A with recorded voltage varying from 19.1 to 29.9 V, and the calculated heat input ranged from 0.37 to 1.11 kJ/mm. Tests were conducted with a preheats of 25, 50, and 100 °C. Similarly, a total of 14 tests were conducted for 10-mm-thick plates under high restraint (R_f=25 mm) with 10 tests instrumented and analysed for cracking results and 4 used to validate the lower limit of weld deposition. The recorded current ranged from 119 to 163 A with the recorded voltage ranging from 21.9 to 24.6 V, and the calculated heat input ranged from 0.48 to 0.82 kJ/mm. Testing was carried out with preheats of 25, 40, and 50 °C.

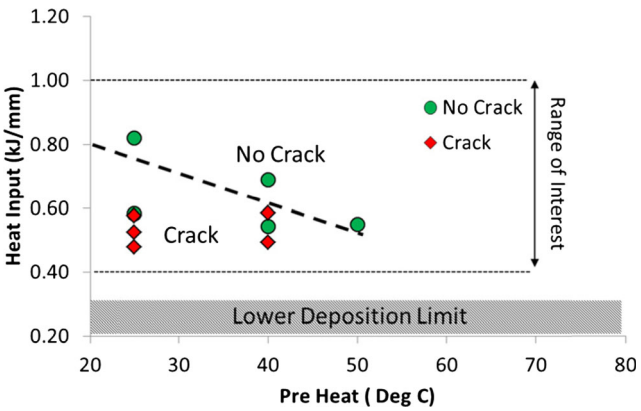

Fig. 10 MWIC weldability testing on the 10-mm-thick API 5 L X70 line pipe steel under high restraint (R_f=25 mm). A *green circle* represents a sample within which no cracking is observed. A *red diamond* represents a sample within which a crack was observed

These weldability tests established a lower heat input (HI) limit of 0.3 kJ/mm for both the 20- and 10-mm tests plates when welded in ambient condition (i.e. $T=25\pm2$ °C and RH <80 %). Below this heat input limit, the welds suffered from insufficient penetration and lack of side wall fusion. Within the heat input range of interest (0.4 kJ/mm < HI < 1 kJ/mm), testing results empirically suggest that for the 20-mm-thick sections of line pipe steel under high restraint (Fig. 9), the minimum (critical) preheat (PH) required to deposit single-pass hydrogen crack-free weld as a function of the heat input can be defined as PH(°C) = 70 − 50 HI(kJ/mm). Similarly, for the 10-mm-thick plates welded under high restraint (Fig. 10), the minimum (critical preheat) required to deposit single-pass hydrogen crack-free welds can be defined as PH(°C) = 100 − 100 HI(kJ/mm).

The observed hydrogen cracks developed on the samples indicated as red triangles in Figs. 9 and 10 can be classified into two distinct categories, macroscopic and microscopic cracks. Macroscopic cracks typically originated from the weld toe and propagated in a transverse fashion though the weld cross section (region of interest (ROI) 1; Figs. 11 and 12). The cracks ranged in length from a tenth of a millimetre to several millimetres. Microcracks, on the other hand, were distributed throughout the weld metal and were generally orientated perpendicular to the forces arising (normal to the weld) as a result of the restraint conditions created by the weldability test specimen. The cracks ranged in length from a fraction of a micrometre to several micrometres. The cracks were also observed to generally initiate from non-metallic inclusion (NMI; Fig. 13). A distinct difference was noted between the number and the severity of the type of cracking observed. For both the

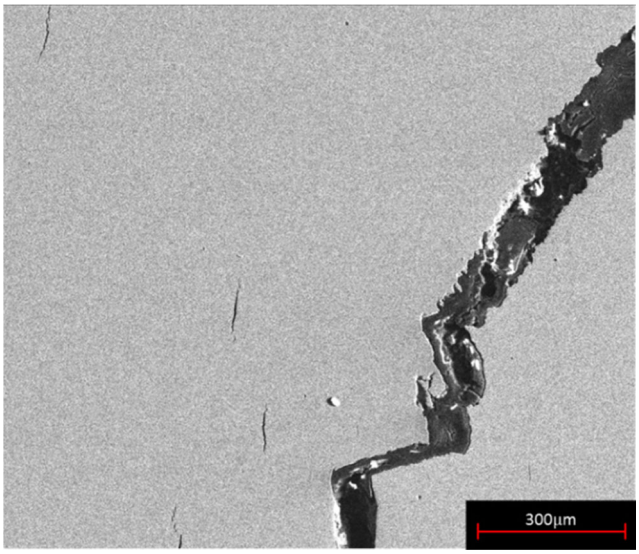

Fig. 12 ROI 1 typical 'macroscopic' hydrogen crack, originating from a stress concentration, typically wagon tracks in the weld toe. The cracks propagate in a transverse fashion towards the weld centreline. 'Microscopic' cracks in the normal direction of the weld can also be observed

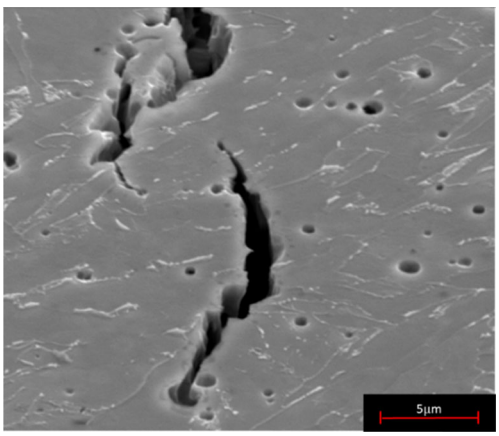

Fig. 13 ROI 2 typical 'microscopic' hydrogen crack. A large proportion of the observed microcracks originated from non-metallic inclusions

20- and 10-mm test plates, there was evidence to suggest than the number of macroscopic cracks increased as the heat input decreased. This could be attributed to the fact that at a lower heat input, the eccentricity of the deposited weld bead increased, creating stress concentrators at the weld toe and thus favourable initiation sites for hydrogen cracks.

At comparable heat input and preheat, the 10-mm plates appeared to have a greater number of microcracks; however, their severity was marginally less than microcracks observed in the 20-mm plates. This may be attributed to the higher overall restraint experienced by the thicker plate.

3.2 Microstructural characterisation

The weld metal samples of both the 10- and 20-mm samples consisted primary of acicular ferrite (Fig. 14a), bainite (Fig. 14b), and Widmanstatten ferrite (Fig. 14c). Some instances of grain boundary ferrite, ferrite with non-aligned second, and ferrite with aligned second phase were also observed. The detailed microstructural analysis of the weld metals is presented in [28]. Given the limited heat input range within which the samples were deposited, it is not surprising that no significant difference was observed in the morphology or fraction of observed microstructures. Additional general review of the microstructure along the macroscopic crack path showed no significant relationship to any particular microstructural morphology [45].

3.3 Micromechanical characterisation

3.3.1 Sample selection

To assess the suitability of micromechanical characterisation as a means of ranking the susceptibility of deposited welds to WMHACC, several samples were selected from across the derived safe welding boundary as highlighted in Figs. 15 and 16.

3.3.2 Weld metal hardness

The weld metal hardness for the 20-mm thick samples ranged from 213.3 to 300 HV for samples welded under

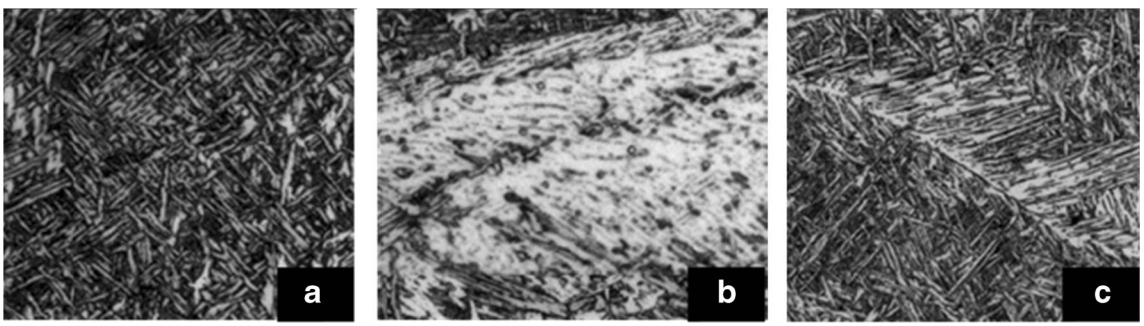

Fig. 14 Micrographs (not scaled) of typical microstructures observed in both the 20- and 10-mm weld metal samples; the samples consisted primarily of acicular ferrite (**a**), bainite (**b**) and Widmanstatten ferrite (**c**)

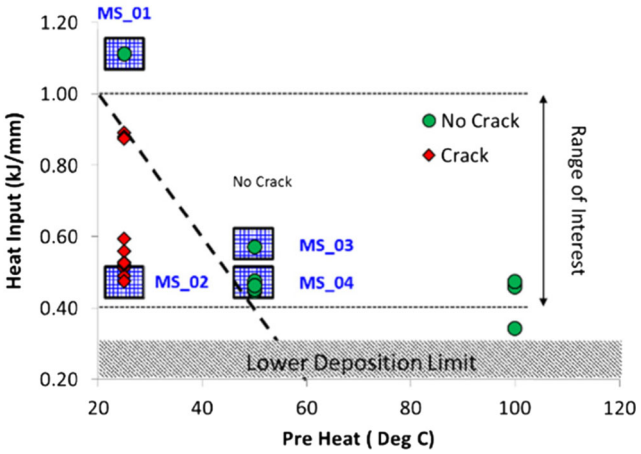

Fig. 15 Samples from the 20-mm test series (grid regions) selected for micromechanical characterisation

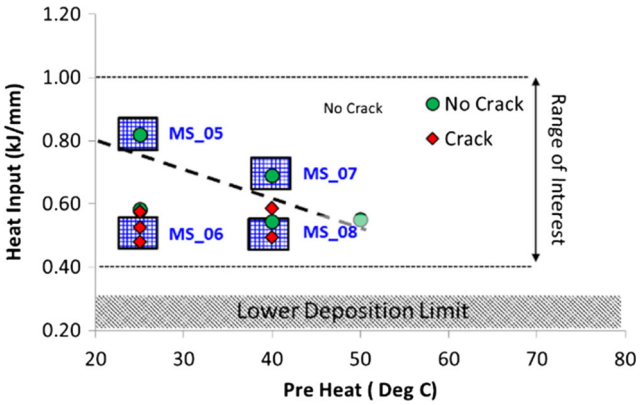

Fig. 16 Samples from the 10-mm test series (grid regions) selected for micromechanical characterisation

ambient conditions and 253.4 to 264.8 HV for samples welded with a preheat of 50 °C (Fig. 17). A maximum standard deviation of 21 HV was recorded across the 20-mm sample set. The variation in the hardness values can be attributed to the different microstructural constituents indented at each test. For 10-mm thick samples (Fig. 18), the measured weld metal hardness ranged from 282.9 to 299.9 HV for samples welded under ambient conditions. The narrow hardness range can be attributed to the narrow heat input range within which the samples were deposited and consequently minimal variation in weld metal microstructure. For samples welded with a preheat of 40 °C, the measured weld metal hardness ranged from 274.9 to 293.5 HV. A maximum standard deviation of 26.1 HV was recorded across the 10-mm sample set.

Considering the measured values of the hardness and their respective standard deviation (Table 5), it can be seen that the preheat and heat input, due to their limited ranges, do not significantly affect the overall hardness values of the weld metals. This is in accordance with the minimal variation of the microstructure observed across the different samples. Nevertheless, two trends can be drawn considering the mean values of the hardness (Table 5). For both the 10- and 20-mm thick samples welded under ambient condition, the hardness tends to decrease with the increase of the heat input due to grain coarsening [46]. At higher preheats, the opposite trend is observed (i.e. the hardness increases with the heat input) for both the 10- and 20-mm samples. This trend, however, may not be significant, considering the experimental scatter of the values

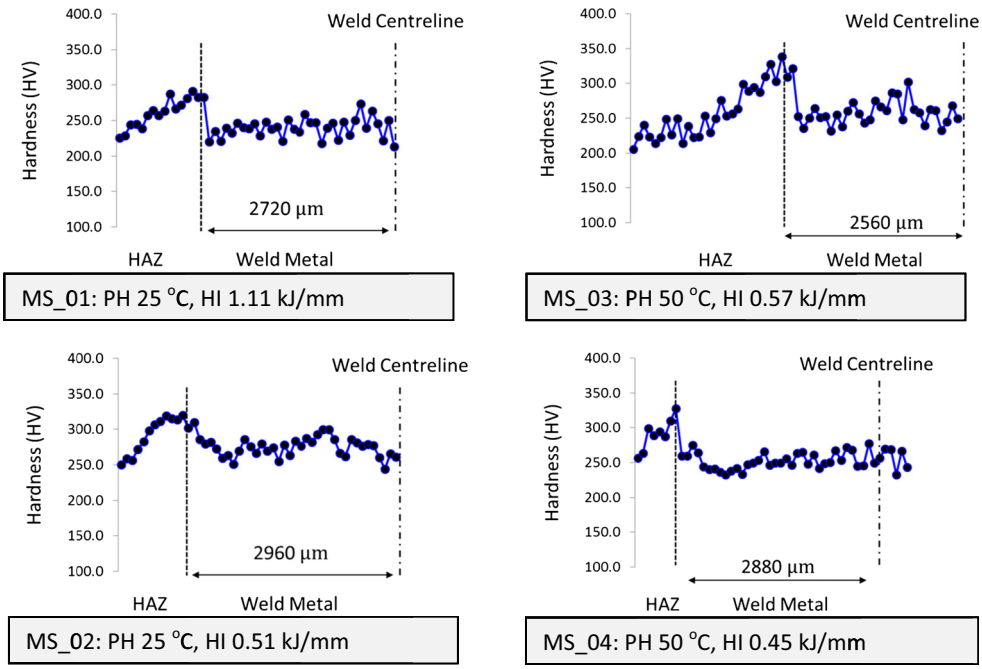

Fig. 17 Hardness traverse for the 20-mm-thick plates

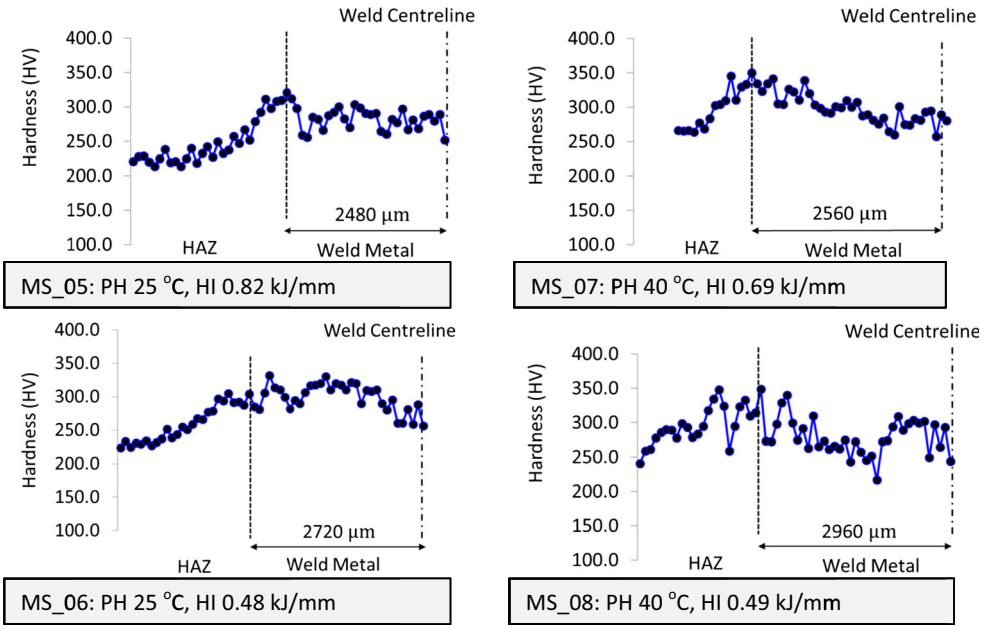

Fig. 18 Hardness traverse for the 10-mm-thick plates

observed within the narrow heat input range used at higher preheats.

Figures 17 and 18 also show that the HAZ hardness increases from the parent metal towards the weld metal fusion zone. The continuous increase of hardness within HAZ may be attributed to the formation of more bainitic structure towards fusion zone as reported for multi-pass welds [47]. In any case, it is important to note that the measured peak hardness through the weld metal and the HAZ did not exceed the generally accepted hardness threshold of 350 HV [29–31], above which hydrogen cracking is expected. Additionally, weld hydrogen cracks were observed in samples with a peak hardness value as low as 300 HV. These observations support the proposition in literature that the traditional empirical hardness limits cannot be used as a universal infallible proxy for hydrogen cracking [3, 4, 14, 16].

3.3.3 Weld metal elastic modulus

The weld metal elastic modulus for the 20-mm thick samples (Fig. 19) ranged from 160 to 182.1 GPa for samples welded under ambient conditions and 169 to 208 GPa for samples welded with a preheat of 50 °C. A maximum standard deviation of 7.4 GPa was noted for the 20-mm data set. The 10-mm data set (Fig. 20) showed a greater degree of variability. For samples welded under ambient conditions, the measured elastic modulus ranged from 142.5 to 203.5 GPa, and for samples welded with a preheat of 40 °C, the measured elastic modulus ranged from 106.3

Table 5 Welding parameters and cracking conditions for samples selected for micromechanical characterisations

	Sample parameters				Hardness (HV)				Elastic modulus (GPa)			
Sample	Heat input (kJ/mm)	Preheat (°C)	Thickness (mm)	Crack/no crack	Maximum	Minimum	Mean	Standard deviation	Maximum	Minimum	Mean	Standard deviation
MS-01	1.11	25	20	No crack	273.4	213.3	242	15.1	182.1	160	170.1	5.4
MS-02	0.51	25	20	Crack	300	244.3	276.7	13.7	181.9	164.4	171.7	4.1
MS-03	0.57	50	20	No crack	338.3	231.7	264.8	21	208.8	180.8	193.5	7.4
MS-04	0.45	50	20	No crack	277.3	232.5	253.4	11.8	186.5	169	178.7	4
MS-05	0.82	25	10	No crack	320.8	251.6	282.9	16.9	161.3	142.5	151.7	4.7
MS-06	0.48	25	10	Crack	331.8	256.7	299.9	20.6	203.5	166.8	189.7	7.6
MS-07	0.69	40	10	No crack	339.4	257.2	293.5	18.4	177.5	158	170.1	4.9
MS-08	0.49	40	10	Crack	340.2	217.1	274.9	26.1	130.4	106.3	121.3	4.9

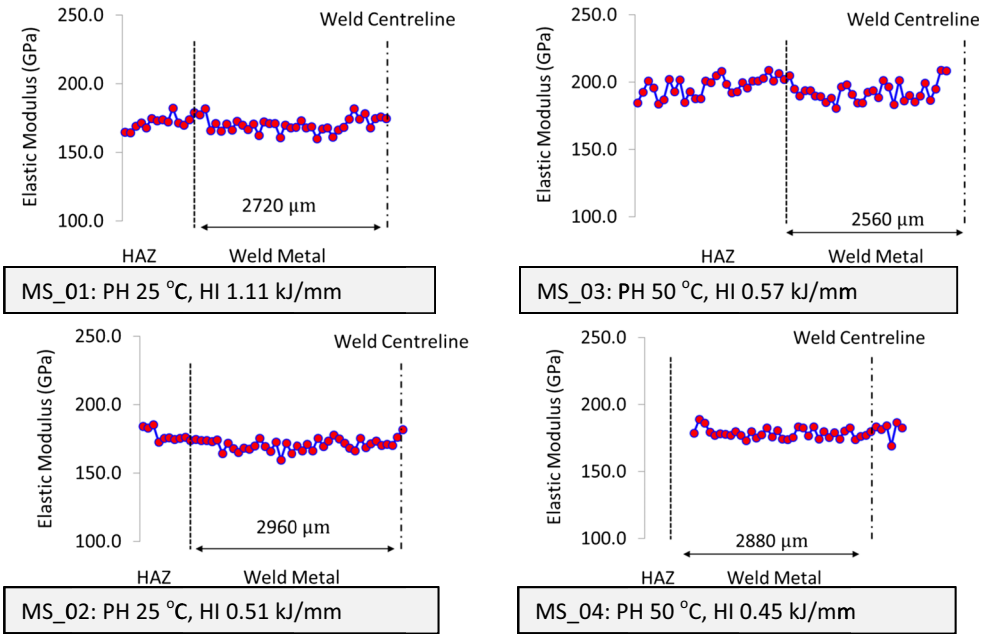

Fig. 19 Elastic modulus traverse for the 20-mm-thick plates

to 177.5 GPa. A maximum standard deviation 7.6 GPa was measured across the 10-mm data set.

The elastic modulus of the considered samples (Table 5) follows the same general trend as the hardness in function of the heat input, i.e. decreases with the increase of the heat input when the samples are welded under ambient condition (that had been observed in [48]) and increases with the increase of the heat input at higher preheat. This latter trend might not be significant though for the reasons evocated in Sect. 3.3.2. Table 5 gathers the welding parameters and the corresponding measured micromechanical properties of the selected samples.

3.4 Proposition of a new proxy for WMHACC susceptibility assessment

Phenomenologically, in order for a hydrogen crack to manifest, a critical concentration of hydrogen needs to be trapped in a susceptible microstructure and subjected to a critical level of stress. For an empirical cracking boundary produced where the only significant difference is the residual hydrogen content in the weld, as influenced by the level of preheat with which the samples were produced [2, 3], it is suggested that this should be some inherent differences in the resulting material

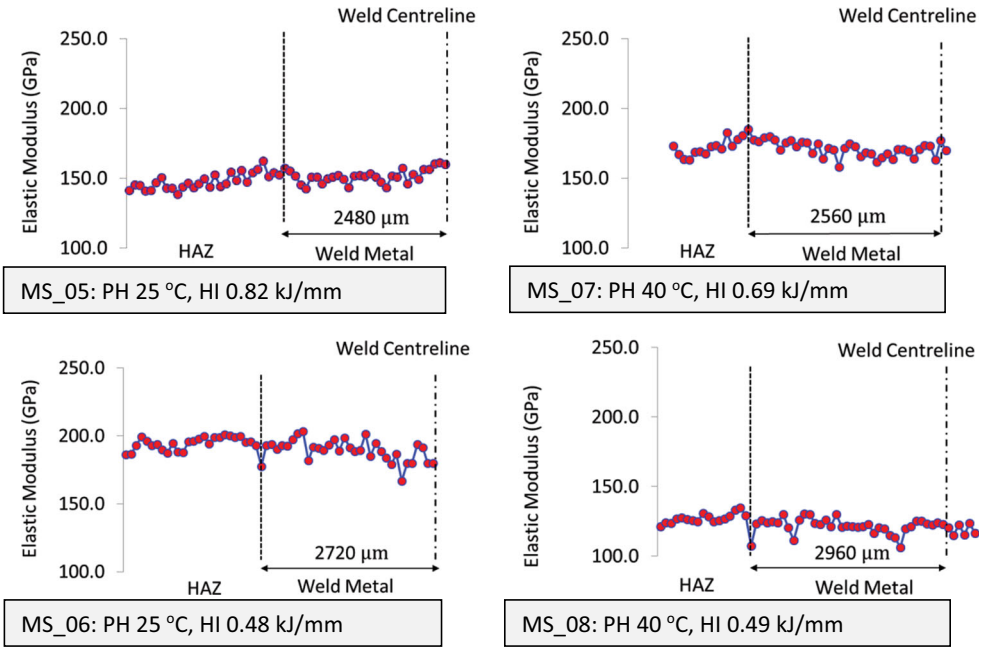

Fig. 20 Elastic modulus for the 10-mm-thick plates

properties across the boundary which allowed for the propagation of a hydrogen crack (for a given preheat).

From the presented results, it seems that the preheat and the heat input affect the hardness and the elastic modulus of the cracked and non-cracked samples in the same directions. However, the samples being situated across an empirical boundary, within narrow heat input ranges, the hardness and elastic modulus do not vary necessarily as expected. Table 5 shows for example that the cracked sample MS-08 has a lower hardness value than the non-cracked sample MS-07 welded at the same preheat but with a lower heat input. Moreover, it has been shown that all cracked samples presented hardness values below the defined threshold of 350 HV below which cracking is not expected. As the propagation of hydrogen cracks is dependent on the elasto-plastic properties of the material within which a crack has initiated [43], it is proposed that the hardness proxy can be refined by combining the hardness with the measured elastic modulus of the material as a ratio hardness/elastic modulus (H/E). This ratio could be used as a more accurate proxy for assessing the susceptibility of a WM to HACC. Moreover, the H/E ratio, traditionally used to rank materials in terms of wear resistance [49–51], appears also in the so-called 'plasticity index' [49, 52], which is widely quoted as a valuable measure in determining the limit of elastic behaviour in a surface contact. Higher H/E values result in higher critical loads for the onset of yield (non-elastic deformation) in indentation [52]. Early works have related the H/E ratio of a material to its yield strength [50, 51], and it has been well established in the literature that the increase of the yield strength decreases the stress intensity threshold for HAC to occur [25–27, 53]. It is thus expected that higher H/E ratio would traduce higher HACC susceptibility of a material.

Examining the ratio of the universal hardness (H in GPa) and elastic modulus (E in GPa) for both the 20- and 10-mm date sets (Figs. 21, 22 and 23), there is evidence to suggest that there is a potential to delineate a boundary which serves as an indicator to the potential susceptibility to WMHACC. The data suggests that if the H/E ratio $>2\times10^{-2}$, the weld is susceptible to WMHACC. Conversely, if the H/E ratio $<1.5\times10^{-2}$, the weld is not susceptible to WMHACC. These experimental outcomes support the hypothesis that materials with higher H/E ratio are more susceptible to HACC. Moreover, it can be seen that the cracked sample MS-08 that could be classified as 'safe' by considering its hardness only (that is lower than the uncracked sample MS-07 for the same preheat but lower heat input) becomes 'unsafe' by considering its H/E ratio (2.3×10^{-2}).The use of the H/E ratio as a refined hardness proxy could be thus a more suitable parameter to predict WMHACC susceptibility than is the hardness alone for HSLA steels.

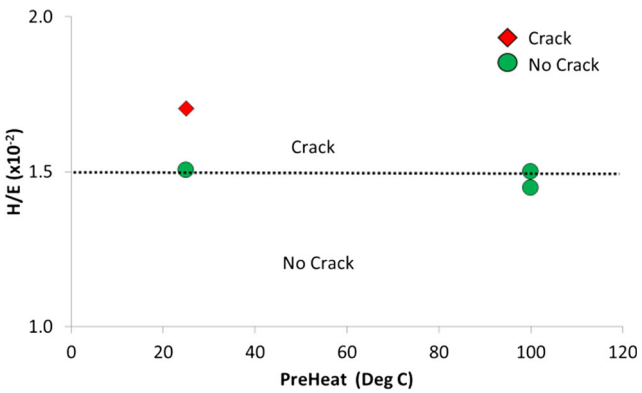

Fig. 21 H/E ratio for samples from the 20-mm data set. No samples with a ratio of $H/E \leq 1.5\times10^{-2}$ cracked

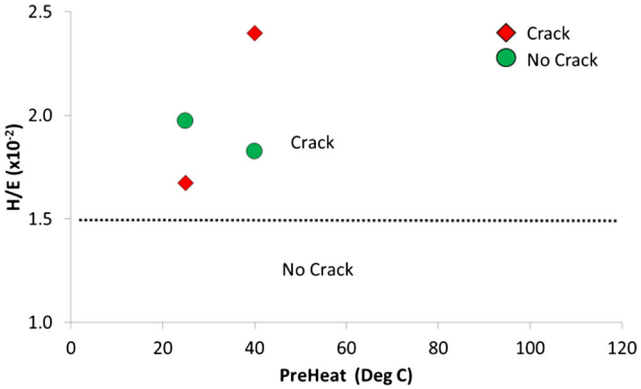

Fig. 22 H/E for samples from the 10-mm data set. A cracking anomaly detected with a ratio of $H/E = 1.6\times10^{-2}$. Uncracked sample has ratio as high as $H/E = 2\times10^{-2}$

3.5 Role of weld bead eccentricity on WHMACC susceptibility

It is important to note that a change in heat input affects not only the thermal cycle of the deposited weld bead but has a profound effect on the geometry of the deposited weld bead, in particular the eccentricity of the weld toe of the deposited weld bead. One potential consequence of a change in bead eccentricity is the distribution of local stresses in the weld

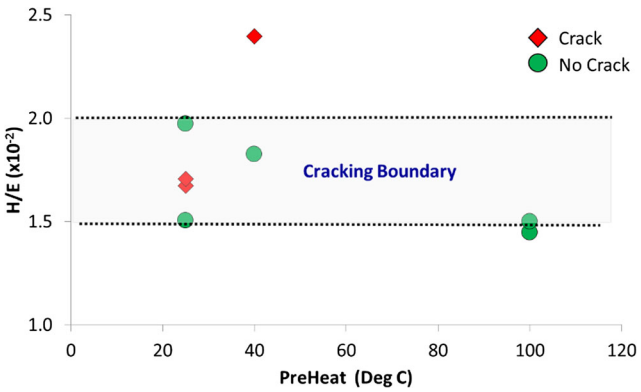

Fig. 23 H/E ratio for both 20 and 10 mm. Combining the data presets a hypothesised boundary within which cracking is uncertain. However, as the yield strain increases, it is postulated that there will be a higher prevalence of WMHACC

bead. This in turn may influence the type and position of hydrogen cracks, given the affinity of atomic hydrogen to areas of high tri-axial stress. It was observed that for the both the 20-mm but especially the 10-mm sample sets, a reduction in the heat input with which a weld was deposited increased the asymmetry of the deposited weld bead. This in turn increased the prevalence cracking in the weld toe. This may be attributed to an increase in the eccentricity of the weld bead profile (Figs. 24 and 25), increasing the intensity of the local stresses at the weld toe, consequently serving as a preferential initiation site for hydrogen cracking.

However, as the preheat levels were increased, the degree of eccentric did not affect the prevalence of cracking as illustrated in Fig. 26. It is therefore suggested that the local weld stresses resulting from bead eccentricity is a critical factor influencing the susceptibility of a single-pass weld to hydrogen cracking.

4 Conclusions

The increased prevalence of WMHACC, as grades of line pipe steel evolve, has raised the question of the reliability of traditional cracking proxies such as hardness. Historically a limit of 350 HV has been established through extensive empirical testing and has been extensively codified.

Empirical testing conducted in this body of work provides data to suggest that the limit of 350 HV does not apply to welds deposited under high restraint, such as those experienced in the pipeline industry during the fabrication of oil and gas transmission and gathering lines.

Welds deposited using E6010 electrodes on two thicknesses (20 and 10 mm) of API 5 L X70 steel at heat inputs ranging from 0.4 to 1.1 kJ/mm were established as having hydrogen cracks in samples with weld metal hardness values as low as 273.4 HV for the 20-mm samples and 331.8 HV for the 10-mm samples.

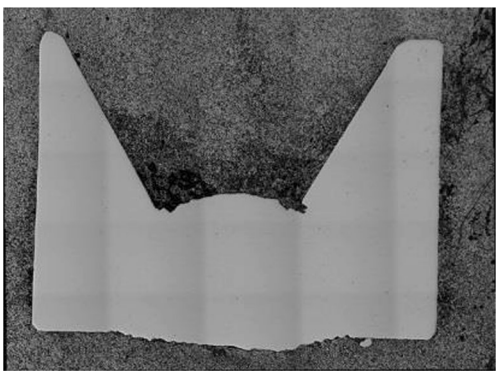

Fig. 24 Typical weld bead geometry for sample deposited with a heat input in the upper quartile of the heat input range of interest. The deposited bead appears symmetrical with no pronounced eccentricity in the weld toe

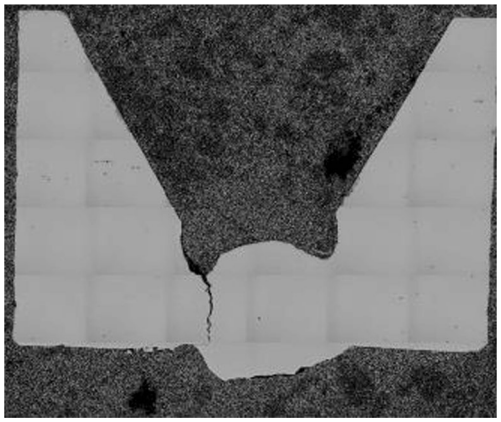

Fig. 25 Typical weld bead geometry for sample deposited with a heat input in the lower quartile of the heat input range of interest. Deposition with a low preheat resulted in the formation of a weld with a produced weld toe and consequently a hydrogen crack

The traditional hardness as a proxy to determine the susceptibility of a WM to HACC proving not to be infallible, and the propagation of hydrogen cracks being dependent on the elasto-plastic properties of the material, it is proposed to refine this proxy by combining the hardness with the elastic modulus of the material as a ratio H/E. From the data collected, this ratio, which is directly related to the yield strength of the material, shows to be a better indicator of the WMHACC susceptibility than is the hardness alone. It is proposed that cracking boundary for API 5 L X70 steel welded with cellulosic electrode is $1.5 \times 10^{-2} < H/E < 2 \times 10^{-2}$.

5 Future work

It is critical to note however that this relationship has been derived based on the empirically testing of one steel composition welded with the same batch of E6010 electrodes for a heat input range typically found in the production of oil and

Fig. 26 Typical weld bead geometry for sample deposited with a heat input in the lower quartile of the heat input range of interest with a heat input of 50°. Despite the irregularity of the weld bead and the eccentric weld toe, no hydrogen cracking was observed in the weld bead

gas pipelines. In order to establish the validity of the predictor for WMHACC in general, it is suggested that a range of steel compositions and electrode combinations are tested for a greater range of heat inputs. This would allow a range of weld metal compositions and microstructural morphologies to be assessed. Although the root pass of a girth weld is accepted as the most vulnerable pass in the welding sequence, to assess the effect of interpass tempering and to ascertain the overall suitability of H/E as a measure of cracking susceptibility, it is also suggested that multi-pass welds be tested.

Acknowledgments The research work was funded by the Energy Pipeline CRC supported through the Australian Government's Cooperative Research Centre Program. The cash and in-kind support from the APGA-RSC is gratefully acknowledged. The authors would also like to thank Neville Cornish from Australian Welding Solutions and Pascal Symons. Walter Costin and Adelaide Microscopy are also acknowledged.

References

1. Barbaro FJ (1999) Types of hydrogen cracking in pipeline girth welds, in: First International Conference on Weld Metal Hydrogen Cracking in Pipeline Girth Welds, Wollongong, Australia, 11.1-11.15. WTIA
2. Yurioka N, Suzuki H (1990) Hydrogen assisted cracking in C-Mn and low alloy steel weldments. Int Mater Rev 35:217–249
3. Kurji R, Coniglio N (2015) Towards the establishment of weldability test standards for hydrogen-assisted cold cracking. Int J Adv Manuf Technol 77:1581–1597
4. Yurioka N (1999) Predictive methods for prevention and control of hydrogen assisted cold cracking. in: First International Conference on Weld Metal Hydrogen Cracking in Pipeline Girth Welds, Wollongong, Australia, 2.1-2.16. WTIA
5. Vasudevan R, Stout RD, Pense AW (1980) A field weldability test for pipeline steels—part II. Weld J 59:76s–84s
6. Signes EG, Howe P (1988) Hydrogen-assisted cracking in high-strength pipeline steels. Weld J 67:163s–170s
7. Fletcher L, Yurioka N (2000) A holistic model of hydrogen cracking in pipeline girth welding. Weld World 44:29–36
8. Beachem CD (1672) A new model for hydrogen-assisted cracking (hydrogen "embrittlement"). Metall Trans 3:437–451
9. Birnbaum HK, Sofronis P (1994) Hydrogen-enhanced localized plasticity—a mechanism for hydrogen-related fracture. Mater Sci Eng A 176:191–202
10. Kinsey AJ (2000) The welding of structural steels without preheat. Weld J 79:79s–88s
11. Fletcher L, Yurioka N (1999) A holistic model of hydrogen cracking in pipeline girth welding. in: First International Conference on Weld Metal Hydrogen Cracking in Pipeline Girth Welds, Wollongong, Australia, 12.1-12.14. WTIA
12. Gedeon SA, Eagar TW (1990) Assessing hydrogen-assisted cracking fracture modes in high-strength steel weldments. Weld J 69: 213s–220s
13. Glover A, Rothwell B (1999) Specifications and practices for hydrogen crack avoidance in pipeline girth welds. in: First International Conference on Weld Metal Hydrogen Cracking in Pipeline Girth Welds, Wollongong, Australia, 13.1-13.18. WTIA
14. Glover A, Graville B (1999) The risk of hydrogen cracking in multipass welds and its effect upon procedure design. in: First International Conference on Weld Metal Hydrogen Cracking in Pipeline Girth Welds, Wollongong, Australia, 9.1-9.23. WTIA
15. Vasudevan R, Stout RD, Pense AW (1981) Hydrogen-assisted cracking in HSLA pipeline steels. Weld J 155s-168s
16. Graville BA, McParlan M (1974) Weld-metal cold cracking. Met Constr Br Weld J 6:62–63
17. Graville BA (1986) A survey review of weld metal hydrogen cracking. Weld World 24:190–198
18. McParlan M, Graville BA (1976) Hydrogen cracking in weld metals. Weld J 55:95s–102s
19. Graville BA (1995) Interpretive report on weldability tests for hydrogen cracking of higher strength steels and their potential for standardization. WRC Bulletin 400
20. Costin WL, Lavigne O, Kotousov A, Ghomashchi R, Linton V (2016) Investigation of hydrogen assisted cracking in acicular ferrite using site-specific micro-fracture tests. Mater Sci Eng A 651C: 859–868
21. Trevisan RE, Fals HC (1999) Fracture modes and acoustic emission characteristics of hydrogen-assisted cracking in high-strength low-alloy steel weldment. J Braz Soc Mech Sci Eng 21:675–682
22. Vuick J (1992) An update of the state-of-the-art of weld metal hydrogen cracking. Weld World 31:308–321
23. Song EJ, Bhadeshia HKDH, Suh DW (2013) Effect of hydrogen on the surface energy of ferrite and austenite. Corros Sci 77:379–384
24. Grabke HJ, Riecke E (2000) Absorption and diffusion of hydrogen in steels. Mater Tehnol 34:331–342
25. Gerberich WW, Chen YT (1973) A threshold stress intensity concept for environmental cracking. Int J Fract 9:369–371
26. Homrossukon S, Mostovoy S, Todd JA (2009) Investigation of hydrogen assisted cracking in high and low strength steels. J Press Vessel Technol-Trans ASME 131:1–11
27. Yamaguchi Y, Nonaka H, Yamakawa K (1997) Effect of hydrogen content on threshold stress intensity factor in carbon steel in hydrogen-assisted cracking environments. Corrosion 53:147–155
28. Ghomashchi R, Costin W, Kurji R (2015) Evolution of weld metal microstructure in shielded metal arc welding of X70 HSLA steel with cellulosic electrodes: a case study. Mater Charact 107:317–326
29. API Standard 1104-Nineteenth Edition (1999) Welding of pipelines and related facilities. American Petroleum Institute, Washington, DC
30. CSA Z662 (2003) Oil and gas pipeline systems, CSA International
31. AS 2885.2-2002 (2002), Pipelines—gas and liquid petroleum, Part 2: welding, Standards Australia
32. Davidson JA, Konkol PJ, Sovak JF (1989) Assessing fracture toughness and cracking susceptibility of steel weldments—a review. WRC Bulletin 345
33. Cheng YT, Cheng CM (1998) Relationships between hardness, elastic modulus, and the work of indentation. Appl Phys Lett 73: 614–616
34. Lucca DA, Herrmann K, Klopfstein MJ (2010) Nanoindentation: measuring methods and applications. CIRP Ann-Manuf Technnol 59:803–819
35. VanLandingham MR (2003) Review of instrumented indentation. J Res Natl Inst Stand Technol 108:249–265
36. Oliver WC, Pharr GM (2004) Measurement of hardness and elastic modulus by instrumented indentation: advances in understanding and refinements to methodology. J Mater Res 19:3–20
37. Chudoba T (2006) Measurement of hardness and Young's modulus by nanoindentation. In: Cavaleiro A, Hosson JT (eds) Nanostructured coatings. Springer, New York
38. Johnson KL (1985) Contact mechanics. Cambridge University Press, Cambridge
39. Fischer-Cripps AC (2000) Introduction to contact mechanics. In: Ling FF (ed) Mechanical engineering series. Springer, New York

40. Maier P, Richter A, Faulkner RG, Ries R (2002) Application of nanoindentation technique for structural characterisation of weld materials. Mater Charact 48:329–339
41. Ye D, Mi F, Liu J, Xu Y, Chen Y, Xiao L (2013) Use of instrumented indentation testing to study local mechanical properties of 304L SS welded joints subjected to low-cycle fatigue loadings. Mater Sci Eng A 564:76–84
42. Fang J, Yuan H (2013) The local concept to assess weldment with help of nano-indentation and FEM simulation, in: 13th International Conference on Fracture. Beijing, China
43. Di Leo CV, Anand L (2013) Hydrogen in metals: a coupled theory for species diffusion and large elastic–plastic deformations. Int J Plasticity 43:42–69
44. Kurji R, et al. (2013) An improved welding institute of Canada test for evaluation of high-strength pipeline steel weldability, Paper no: S11-03, 6th International Pipeline Technology Conference, Ostend, Belgium
45. Costin WL, Lavigne O, Linton V, Brown IH, Kotousov AG, Barbaro FJ, Ghomashchi R (2013) Micromechanical examination of the relationship between weld metal microstructure and hydrogen assisted cold cracking, Paper no: S10-02, 6th International Pipeline Technology Conference, Ostend, Belgium
46. Kumar S, Shahi AS (2011) Effect of heat input on the microstructure and mechanical properties of gas tungsten arc welded AISI 304 stainless steel joints. Mater Des 32:3617–3623
47. Alipooramirabad H, Ghomashchi R, Paradowska A, Reid M (2016) Residual stress-microstructure-mechanical property interrelationships in multipass HSLA steel welds. J Mater Process Technol 231:456–467
48. Rafiqul MI, Ishak M, Rahman MM (2011) Effects of heat input on mechanical properties of metal inert gas welded 1.6 mm thick galvanized steel sheet. IOP Conf Ser: Mater Sci Eng 36:1–8
49. Leyland A, Matthews A (2000) On the significance of the *H*/*E* ratio in wear control: a nanocomposite coating approach to optimised tribological behaviour. Wear 246:1–11
50. Oberle TL (1951) Properties influencing wear of metals. J Metals 3: 438–439
51. Finkin EF (1974) Examination of abrasion resistance criteria for some ductile metals. J Tribol-Trans ASME 96:210–214
52. Zhang S (2016) Thin films and coatings—toughening and toughness characterization. CRC Press, Taylor and Francis Group, Boca Raton
53. Loginow AW, Phelps EH (1975) Steels for seamless hydrogen pressure vessels. Corrosion 31:404–412